Sensitivity Analysis of Mixing Front Control between Saline and Fresh Groundwater in the Marvdasht-Kharameh Aquifer Using the MODPATH-MODFLOW Model

Shahin Tavallali
Ferdowsi University of Mashhad
Mahmoud Maghrebi
magrebi@yahoo.com
Ferdowsi University of Mashhad https://orcid.org/0000-0002-0082-0020
Mohammad Taghi Dastorani
Ferdowsi University of Mashhad

Research Article

Keywords: Sensitivity Analysis, MODPATH-MODFLOW Model, Saline and Fresh Groundwater Interface, Marvdasht-Kherameh Aquifer

Posted Date: May 15th, 2025

DOI: https://doi.org/10.21203/rs.3.rs-6484900/v1

Sensitivity Analysis of Mixing Front Control between Saline and Fresh Groundwater in the Marvdasht-Kharameh Aquifer Using the MODPATH-MODFLOW Model

Shahin Tavallali[1], Mahmoud F. Maghrebi[2], Mohammad Taghi Dastorani [3]*

[1]Ph.D. candidate, Faculty of Natural Resources and Environment, Ferdowsi University of Mashhad, Iran

[2] Professor of Civil Engineering Department, Ferdowsi University of Mashhad, 91775-1111, Iran

[3] Professor, Faculty of Natural Resources and Environment, Ferdowsi University of Mashhad, Iran

[*] (Corresponding author) Email: maghrebi@um.ac.ir

Abstract

This study analyzes the sensitivity of groundwater flow and the mixing fronts of saline and fresh transient groundwater in the Marvdasht-Kherameh aquifer using the MODPATH-MODFLOW model. In groundwater flow modeling, IPCC scenarios (such as RCPs and SSPs) are used to predict climate changes, including variations in temperature and precipitation, which can directly impact groundwater levels, aquifer recharge, and groundwater flow patterns. Uncertainty analysis was conducted using the First-Order Reliability Method (FORM) to assess the aquifer's sensitivity to groundwater level changes. The findings indicate that the flood volume entering water bodies diminishes during wet and dry periods as it mixes with saline water. The critical scenario involves water infiltration into the aquifer, highlighted by FORM results, showing a homogeneous flow pattern in the affected region. Excessive groundwater extraction has led to significant flow disruption risks in concentrated healthy areas. Saline water infiltration from the wetland and lake accelerates desiccation. It maintains stable flow in the southeastern plain, leading to salt accumulation and destruction of the aquifer's recharge structure in central regions. Effective management strategies are necessary to preserve the region's ecological and hydrological balance. This research provides valuable insights into the interactions between saline and fresh groundwater and their impact on aquifer stability and wetland health.

Keywords: Sensitivity Analysis, MODPATH-MODFLOW Model, Saline and Fresh Groundwater Interface, Marvdasht-Kherameh Aquifer

1. Introduction

Increasing challenges such as climate change, excessive groundwater extraction, and pollutant intrusion profoundly impact the delicate balance between saline and fresh groundwater fronts. These environmental and human-induced changes often lead to the displacement and mixing of these fronts, jeopardizing groundwater resources' quality and availability (Roy & Datta, 2020; Sharma et al., 2021). Given the complexity of these dynamics, traditional groundwater management approaches often fail to provide accurate and effective solutions (Amanambu et al., 2020). The mixing front refers to the interface where saline and fresh groundwater meet and interact within an aquifer. This front plays a crucial role in determining groundwater quality, especially in areas where salinity intrusion is a concern. The movement and extension of the mixing front are influenced by several factors, including aquifer recharge, extraction rates, and external saline sources. In this study, we focus on how the mixing front behaves and extends, particularly under varying climatic and extraction scenarios in the Marvdasht-Kherameh aquifer.

This is where sensitivity analysis becomes indispensable. By identifying critical parameters and quantifying their impact on the system's behavior, sensitivity analysis helps better understand the hydrodynamic processes governing groundwater flow (Ghadeer & Maghrebi, 2023; Vatanchi & Maghrebi, 2022). Moreover, it enables more precise predictions of how various factors, such as changes in climate or extraction rates, affect groundwater quality and availability (Cao et al., 2020; Moutsopoulos, 2021). Therefore, sensitivity analysis not only enhances modeling accuracy but also informs decision-making, such as the optimal placement of wells, artificial recharge systems, and the evaluation of development projects (Pargar et al., 2024; Tareghian et al., 2024). Through these applications, sensitivity analysis offers a path to more efficient and sustainable management of groundwater resources, particularly in regions facing severe water scarcity (Mohammadi et al., 2021; Ma et al., 2024; Boni et al., 2020).

Zhang et al. (2010) evaluated pollutant concentration levels in an airport area using the probabilistic reliability assessment method (PRAM). Sensitivity analysis helps quantify and assess different factors' contribution to the overall uncertainty in model predictions. Still, uncertainty can arise from various sources, including measurement errors, parameter estimation, model structure, and external factors.

Iqbal et al. (2018) investigated the effects of groundwater pumping and river bank filtering (RBF) on the installation of wells, pumping rates in flow paths, travel time, pumping size, determining coverage area, and mixing of groundwater in a pumping well in the Penang region, Malaysia. The results indicated that river water movement to the aquifer is generally slow, depending on pumping rates and the well's distance from the river. Alimonti et al.

(2017) conducted an uncertainty analysis using a reliability assessment to quantify soil variability. Using the First-Order Reliability Method (FORM), the reliability index and failure probability demonstrated a practical and straightforward method for simultaneous implementation. Their work analyzed the potential effects of aquifer compaction in the Scarlino plain of Italy resulting from the expansion of hydraulic barriers for water reclamation. Dey and Prakash (2022) stated that coastal areas are densely populated due to social and economic benefits, increasing the demand for fresh water. Coastal aquifers acting as large freshwater reservoirs can meet this growing demand. Performance evaluation results indicate the method's application for managing saltwater intrusion while maximizing freshwater pumping in coastal aquifers. Feo et al. (2018) mentioned that the MODFLOW model is currently the most popular tool for studying groundwater flow and aquifer modeling. To simplify the MODFLOW interface, Graphical User Interfaces (GUIs) are used to create model definition files and visualize and interpret results (Baradaran and Ameri 2023; Ayar et al. 2022). They developed the FloPy interface for MODFLOW, allowing users to import and utilize simulation data generated using Python.

Considering these challenges, this study investigates how sensitivity analysis can be applied to groundwater modeling, specifically addressing key scientific questions such as the role of aquifer diffusion coefficients in long-term groundwater flow predictions and the effects of recharge projects on salinity levels. The study aims to advance the understanding of how these factors interact and contribute to groundwater management strategies (Doherty 2001; Feo et al. 2018). The primary innovation of this research lies in the integration of advanced probabilistic methods (Alimonti et al. 2017; Dey and Prakash 2022), such as FORM uncertainty analysis, with GIS-based spatial modeling to evaluate the dynamic behavior of aquifer diffusion coefficients over extended periods. While methods for creating continuous raster maps exist, this study introduces a novel approach by combining these techniques with the MODFLOW and MODPATH models to enhance the accuracy of long-term predictions and optimize groundwater resource management strategies, particularly in regions vulnerable to salinity intrusion.

2. Materials and Methods

2.1. Study Area Introduction

The Marvdasht-Kharameh study area is in Fars Province, Iran, covering 3926.1 km^2, including 1823.4 km^2 of highlands and 2102.7 km^2 of plains (Raja et al. 2019). This area consists of six plains: Dashtak-Doroodzan, Mayin-Bidkal, Ramjerd, Dashtbal-Laneh Tavous, Marvdasht-Karbal, and Kharameh. The Marvdasht-Kharameh study area

contains an alluvial aquifer with a total area of 1470.5 km^2, playing a crucial role in the groundwater supply for the region (Ahmadi Akhormeh et al. 2015). This aquifer is divided into two main sections: the Marvdasht aquifer (1221.5 km^2) and the Kharameh aquifer (249 km^2). To measure the depth and level of groundwater in this area, water level measurements have been conducted in 72 observation wells (Ahmadi Akhormeh et al. 2015; Baradaran et al. 2024). These measurements began in the 1991-1992 water year for the Kharameh Plain, 2000-2001 for the Marvdasht-Karbal Plain, and 2003-2004 for the other plains. Figure 1 shows the geography of the study area and illustrates the location of the observation wells drilled in the Marvdasht-Kharameh aquifer area by the black point on the aquifer surface.

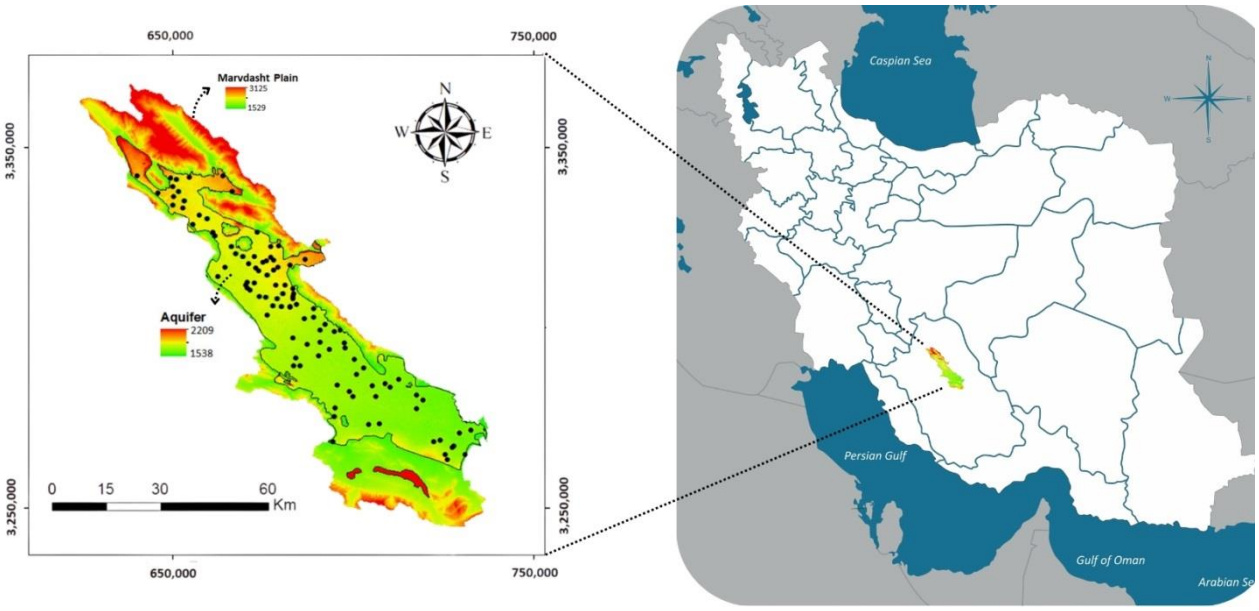

Figure 1. The geographical location of the Marvdasht-Kharameh study area with the location of observation wells (black points)

2.2. Numerical Modeling

The Groundwater Modeling System (GMS) software is one of the most advanced tools for groundwater modeling, developed by Aquaveo (Samani 2024). This software offers extensive capabilities, including modeling groundwater flow using models like MODFLOW, pollutant transport analysis with models such as MT3DMS and RT3D, and particle tracking with the MODPATH model (Mohammed et al. 2023). GMS allows for importing and processing geological, hydrological, and hydrogeological data and utilizes advanced graphical tools for data visualization and results interpretation. The software can create complex three-dimensional models and conduct sensitivity analyses

and calibrations. Additionally, GMS has powerful capabilities for simulating the impacts of human activities, such as agriculture, industry, and urbanization, on groundwater resources and provides management solutions to preserve and improve water quality (Amiri et al. 2023; Yazdi et al. 2024).

One of the essential and widely used models in GMS is the MODPATH model, which tracks particle paths in groundwater environments (Alaviani et al. 2018). MODPATH is a particle-tracking model that operates based on the results of flow models like MODFLOW. This model uses hydrodynamic data and boundary conditions to simulate the movement paths of particles in groundwater environments. In MODPATH, hypothetical particles are placed at various points in the model, and their paths are tracked based on water flow. This method allows researchers to predict groundwater pollutants' paths and travel times (Alaviani et al. 2018). The capabilities of the MODPATH model include simulating particle paths in complex flow systems, analyzing forward and backward tracking paths, and evaluating particle travel times. This model can help identify areas vulnerable to pollution, determine its sources, and spread assessments. MODPATH is also helpful in groundwater resource management analyses, as it can evaluate the effects of water extraction, water injection, and other management activities on groundwater distribution and movement (Ghandehari et al. 2024).

The combination of GMS's advanced capabilities and various models, including MODPATH, makes this software a robust and comprehensive tool for analyzing and managing groundwater resources. GMS and its diverse models help researchers and water resources managers analyze and manage complex groundwater issues with high accuracy and efficiency. In particular, the ability of the MODPATH model to accurately track particle paths and predict pollutant spread provides a critical tool for protecting groundwater quality and developing effective management strategies (Amiri et al. 2023; Alaviani et al. 2018; Ghandehari et al. 2024). This study used the MODPATH-MODFLOW model to analyze the sensitivity of controlling the mixing cycles of saline and fresh groundwater fronts in the Marvdasht-Kharameh aquifer. The input parameters for the model are presented in Table 1.

To accurately simulate the mixing front between saline and fresh groundwater, the boundaries of the mixing front were defined using salinity gradients within the aquifer. The movement and extension of the mixing front were tracked through the MODFLOW and MODPATH models, which were employed to simulate groundwater flow and particle transport respectively. These models incorporate several key parameters, including hydraulic conductivity, recharge rates, and groundwater extraction rates. The boundaries of the mixing front were dynamically simulated by evaluating salinity concentrations across the aquifer grid at various time intervals. The model results show that the

mixing front shifts in response to seasonal variations in recharge and changes in extraction rates. This dynamic behavior was captured by the combination of MODFLOW's flow modeling and MODPATH's particle tracking capabilities, which allowed us to simulate the movement and dispersion of the saline and fresh groundwater interface.

Table 1. Primary and secondary parameters used in numerical modeling

Data Type	Primary Model Parameters	Secondary Model Parameters	Source
Topography	Digital elevation maps of the region	Slope maps and directions	(Akter and Ahmed 2021)
	Topology maps of the region	Finite difference grid of surface features	
Remote Sensing	MODIS satellite images	Vegetation cover maps and other data	(Mokarram et al. 2022)
Soil	Soil permeability data (K)	Estimation of hydraulic conductivity in the plain	
Geology	Geological maps of the study area	Drawing and refining transmissivity contour lines	(Ahani and Noshadi 2019)
	Aquifer bedrock layer	Interpolated contour lines on the finite difference grid of the aquifer bedrock	
	Well logs	-	
	Geophysical data from consultants	-	
	Aquifer basin boundary spatial layer and saturated aquifer boundary	Precise determination of boundary conditions	(Mokarram et al. 2022)
Land Use	Land use maps	Detailed land status and changes over time	(Heydari and Jabbari 2022)
Meteorology	Rainfall data	Isohyet maps	
	Evapotranspiration data	Iso-evapotranspiration maps	(Ahani and Noshadi 2019)
	Surface runoff input and output data within the plain	Refinement of transmissivity values, water levels, and river network bed	(Heydari and Jabbari 2022)
Hydrogeology	Observation well data	Flow path determination using the Kriging method	(Mokarram et al. 2022)
	Extraction well data	-	
	Input and output flows at reservoir sites or recharge basins	Precise determination of boundary conditions	(Ahani and Noshadi 2019)
	Aquifer storage coefficient	SS	
	Specific yield estimation of unconfined aquifer	SY	
Water Quality	EC data from wells	Refining areas with salinity issues and problem-free zones	(Raja and Parsinejad 2023)
Human Activities	Construction points for dams and canals	-	(Ahani and Noshadi 2019)

It is important to understand the distinction between primary and secondary model parameters, as this distinction plays a crucial role in how the model is built and how accurately it simulates the system.

Primary parameters are the core physical characteristics of the system that directly influence the modeled processes. They form the foundation of the model and are essential for constructing the simulation. Primary parameters include

142 factors such as soil permeability, aquifer properties, and elevation maps. These parameters directly affect the main
143 dynamics being studied, such as the movement of water or materials, and are integral to the functioning of the
144 model. Without accurate primary data, the model's ability to represent the system accurately would be compromised.
145 In contrast, secondary parameters are derived from the primary data and help to enhance the model's accuracy or
146 simulate specific phenomena that are not directly tied to the core processes. These parameters provide additional
147 context and detail to the simulation. For example, land use maps, rainfall data, and water quality data are considered
148 secondary parameters. While they are essential for improving the model's precision and understanding the broader
149 environmental influences, they do not directly drive the core processes of the system being modeled. Essentially,
150 secondary parameters enrich the model, providing a more complete picture, but they are not critical to its
151 fundamental structure.
152 By distinguishing between these two types of parameters, the model can more effectively simulate the real-world
153 system, ensuring that primary factors govern the key dynamics while secondary factors provide additional context
154 for accuracy and specificity.

155 **2.3. Kriging Interpolation**

156 Spatial zonation was performed using the Kriging interpolation method in GIS software. First, the particle travel
157 distances for each coordinate were determined. These data were then used as input for the Kriging model. Kriging is
158 an advanced interpolation technique that estimates values at unknown points based on measured values at known
159 points, considering spatial correlations and the variogram structure. Due to its ability to model spatial variations,
160 Kriging was an ideal choice for zonation and detailed particle distribution analysis in complex environments.
161 Kriging enabled a more accurate simulation of spatial particle dispersion and creating spatial zonation maps,
162 significantly contributing to subsequent analyses and management decisions. In Kriging interpolation, the prediction
163 of the unknown value at a location x_0 is given by a weighted sum of the known values (Eq. 1).

$$\hat{Z}(x_0) = \sum_{i=1}^{n} \lambda_i Z(x_i) \quad (1)$$

164

165 where $\hat{Z}(x_0)$ is the predicted value at x_0, $Z(x_i)$ is the known value at x_i, λ_i is the weight associated with the known
166 value at x_i, and n is the number of known data points. The weights λ_i are determined by minimizing the estimation
167 variance subject to the constraint that the estimator is unbiased. This leads to the system of linear equations (Eq. 2):

$$\sum_{j=1}^{n} \lambda_j \, \gamma(x_i, x_j) + \mu = \gamma(x_i, x_0) \quad , \quad i = 1, 2, ..., n \tag{2}$$

where $\gamma(x_i, x_j)$ is the semivariance between the points x_i and x_j, and μ is a Lagrange multiplier used to enforce the unbiasedness constraint.

2.4. *R*-squared

R^2 measures the proportion of the variance in the dependent variable that is predictable from the independent variables in a regression model. It is also known as the coefficient of determination and is widely used to evaluate the goodness of fit in regression analysis (Eq. 3).

$$R^2 = 1 - \frac{SS_{res}}{SS_{tot}} \quad , \quad SS_{res} = \sum_{i=1}^{n} (y_i - \hat{y}_i)^2 \quad , \quad SS_{tot} = \sum_{i=1}^{n} (y_i - \bar{y})^2 \tag{3}$$

where SS_{res} (Residual Sum of Squares) is the sum of the squared differences between the observed values and the predicted values from the model, and SS_{tot} (Total Sum of Squares) is the sum of the squared differences between the observed values and the mean of the observed values. It should be noted that y_i is the observed value and $\hat{y}_i$ is the predicted value from the regression model, and $\bar{y}$ is the mean of the observed values.

2.5. FORM (First-Order Reliability Method)

The First-Order Reliability Method (FORM) is a foundational technique in structural and engineering reliability analysis used to evaluate the probability that a system will fail under given uncertainties (Liu et al. 2023). The method transforms the input variables, often uncertain or random, into a standard normal space, making the complex problem more manageable. This design point is found through an optimization process, where the method linearizes the limit state function at this critical location (Hu et al. 2023). FORM is precious in scenarios where direct simulation methods, like Monte Carlo simulations, would be too computationally expensive. Due to its balance between computational efficiency and accuracy, it is extensively used in various engineering fields, including civil, mechanical, and aerospace engineering. However, its reliability can decrease for problems involving highly nonlinear behaviors or multiple failure modes, where more sophisticated or higher-order methods might be necessary. Despite its limitations, FORM remains a cornerstone in reliability analysis for engineering design and risk assessment. The key formula (Eq. 4) for the FORM is the expression for the probability of failure P_f, which is based on the reliability index β:

$$P_f = \Phi(-\beta) \quad (4)$$

where Φ is the cumulative distribution function (CDF) of the standard normal distribution, and β is the reliability index, representing the distance from the origin to the limit state surface in standard normal space.

3. Model Calibration and Validation

In this study, the Marvdasht-Kharameh aquifer model was developed to simulate groundwater flow and assess the sensitivity of saline and fresh groundwater fronts. The model was created using the Groundwater Modeling System (GMS) software, which offers advanced capabilities for groundwater modeling, including MODFLOW for flow simulation and MODPATH for particle tracking. After the model design and data input, calibration and validation were performed to ensure accuracy in predicting future aquifer behavior under various conditions.

The data input for the model was sourced from multiple datasets. Topographic data were represented by digital elevation maps (DEM), which were used to simulate surface features and define the spatial distribution of the groundwater system. Soil permeability and geological maps of the study area were used to characterize the hydrogeological properties of the aquifer. Observational data for groundwater levels, precipitation, and evapotranspiration were gathered over 127 months to model seasonal and long-term variations. Furthermore, MODFLOW and MODPATH models were employed to simulate groundwater flow and the movement of particles in the aquifer. Boundary conditions were defined using regional hydrogeological data to represent the aquifer boundaries and recharge zones.

The model calibration was conducted over 127 months. The primary objective was to adjust parameters such as hydraulic conductivity (K) and other hydrogeological factors to match the model's outputs with observed data. This process involved iterative adjustments to minimize discrepancies between simulated and observed groundwater levels. Parameters were calibrated for each aquifer layer, ensuring accurate groundwater flow simulations. The calibration process was continually refined by incorporating updated observational data. Figure 2 compares observed and simulated head values, confirming the model's calibration accuracy.

For model validation, observational data from the last 31 months of the 127-month study period were used, providing an independent dataset for testing the model's predictive accuracy. The model successfully simulated the future behavior of the aquifer, showing good agreement with observed data. The comparison between simulated and

observed groundwater levels demonstrated that the model could replicate real-world conditions effectively. In addition, the R^2 values presented in Table 2 reflect the high accuracy of the model in simulating aquifer behavior.

Table 2. R-squared reduction in the validation stage of the Marvdasht-Kharameh plain model

Property	Value
Mean Residual (Head)	-0.92 (m)
Mean Absolute Residual (Head)	1.86 (m)
Root Mean Squared Residual (Head)	0.92 (m)
Mean Residual (Flow)	0 (m^3/s)
Absolute Residual (Flow)	0 (m^3/s)
Root Mean Squared Residual (Flow)	0 (m^3/s)
Mean Weighted Residual (Head+Flow)	0 (m^3/s)
Mean Absolute Weighted Residual (Head+Flow)	0 (m^3/s)
Root Mean Squared Weighted Residual (Head+Flow)	0 (m^3/s)
Sum of Squared Weighted Residual (Head+Flow)	0 (m^3/s)
Displayed Precision	2

In this study, both primary and secondary model parameters were utilized to enhance model accuracy. Primary parameters are the fundamental physical characteristics of the system, such as soil permeability, aquifer properties (like hydraulic conductivity), and elevation maps, which directly influence the model's behavior. Secondary parameters, derived from the primary data, were used to refine the model or simulate specific phenomena. For example, land use maps, rainfall data, and water quality data (such as EC data from wells) were used to improve the simulation of the aquifer's behavior, particularly in assessing human impacts and groundwater quality.

The results of the calibration and validation processes indicate that the model has successfully simulated groundwater level fluctuations with high accuracy (Figure 2a). The residual error analysis shown in Figure 2b confirms that the model's predictions are close to observed values, with minimal error. This demonstrates the model's ability to predict aquifer behavior reliably, even in the validation stage. In conclusion, calibrated and validated with primary and secondary parameters, the model has been proven to simulate groundwater behavior in the Marvdasht-Kharameh aquifer accurately. This model can be a reliable tool for analyzing and forecasting future aquifer conditions and supporting decision-making in water management strategies.

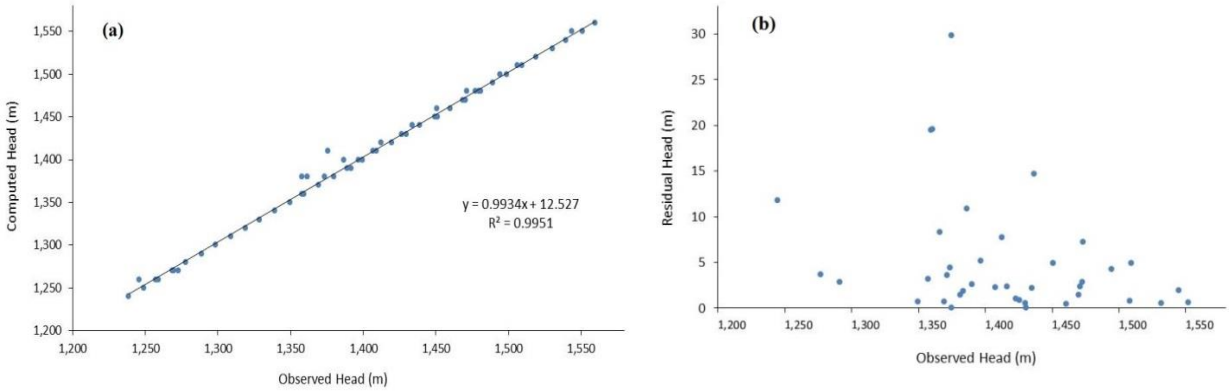

Figure 2. (a) A comparison between the predicted head and the observed value, and (b) Residual error of calculated values versus validation observation data

4. Results and Discussion

The mixing front in the Marvdasht-Kherameh aquifer exhibits dynamic behavior in response to varying conditions of groundwater extraction, recharge rates, and seasonal variations. Figure 3 presents the tolerance zones of the aquifer, categorizing regions into high-risk (red) and low-risk (blue) areas based on their susceptibility to saline intrusion and the movement of the mixing front. The red zones, representing areas of higher vulnerability, show rapid extension of the mixing front towards the freshwater zones during periods of increased groundwater extraction. This phenomenon is most evident in the southeastern regions, where higher extraction rates and reduced recharge exacerbate salinity intrusion, shifting the mixing front inland. In contrast, the blue zones, indicating stable conditions, show limited movement of the mixing front, as these areas are either less affected by saline intrusion or experience more consistent recharge, keeping the boundary of the mixing front relatively stable. Our model simulations confirm these observations, with significant shifts in the mixing front observed during dry periods and high extraction rates. These findings highlight the importance of managing groundwater extraction to prevent the rapid encroachment of saline water into freshwater zones.

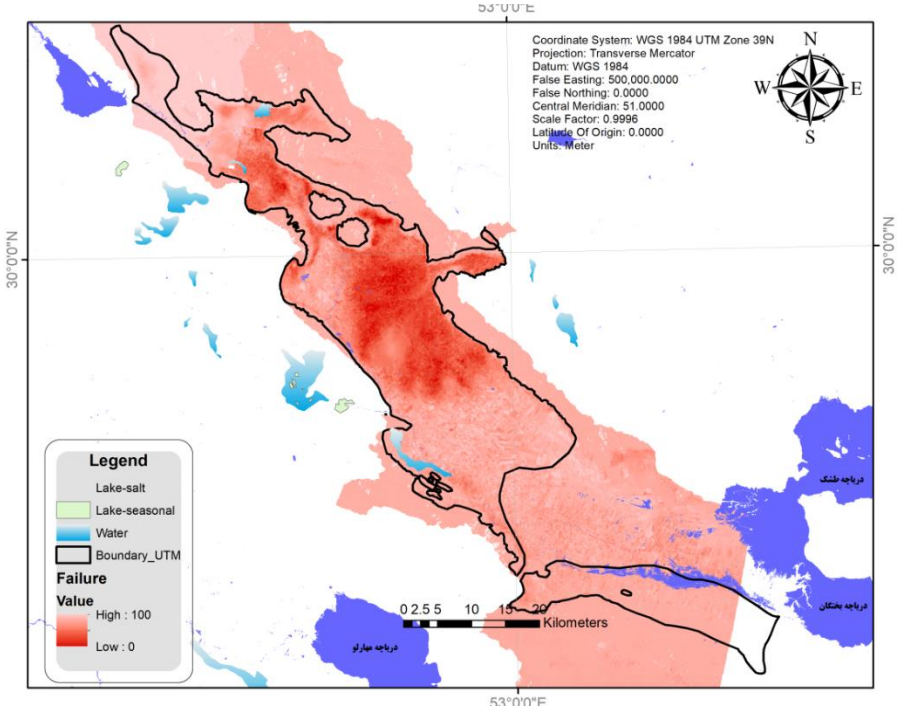

Figure 3. Tolerance zoning graph of saturated aquifer areas.

250

251 **4.1. Model Output Balance**

252 One of the most critical factors affecting the determination of the routing map, synonymous with the concept of the
253 dispersion coefficient, is the flow budget. This concept, developed by the USGS (United States Geological Survey)
254 for calculating the water balance in the MODFLOW model, is crucial. The results obtained from the Flow Budget
255 applied in the calibrated MODFLOW model show that, on average, a specific share of the fixed aquifer storage
256 decreases daily during the 127-month simulation period (Figure 4). This reduction, considering the decline in the
257 groundwater level in the Marvdasht-Kherameh aquifer, is equivalent to a reservoir deficit of over ten years (Figure
258 3a). Changes in the volume of in and outflow from the total boundaries (see Figure 1) with continuous loads are
259 shown in Figure 4a, and the volume of recharge and discharge flows from the river networks are shown in Figure 4b

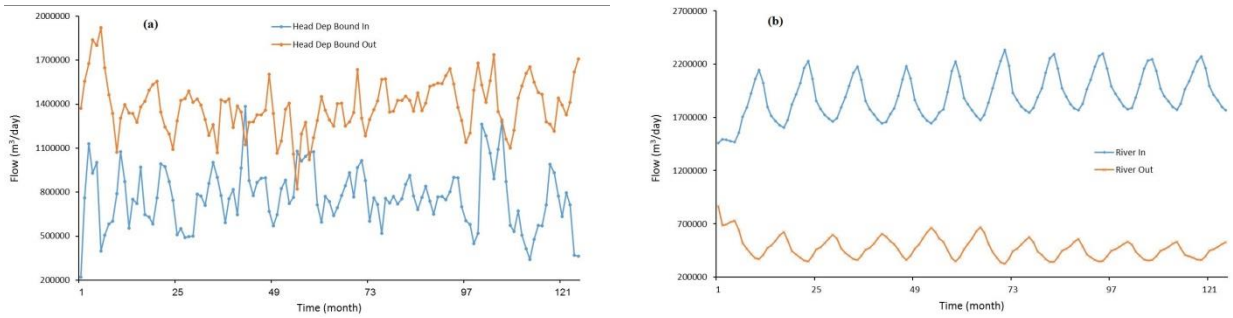

Figure 4. (a) The inflow and outflow from dynamic boundaries and (b) the volume of recharge and discharge from river networks in the Marvdasht-Kharameh plain.

In analyzing the Head Dep Bounds parameter shown in Figure 4a, it is necessary to state that this flux is defined at the boundaries of each border cell, with changes in the head of in and outflows to that cell, considering the relevant head and dependent drainage boundary, as specified in the software packages. This flux is expressed in the software output. Figure 4b shows the groundwater inflow (recharge) volume to the aquifer area under study, including groundwater inflow from the highlands. In Figure 4b, the outflow (discharge) volume from the study area's river network shows no permanent river (red path). Thus, the outflow volume from the plain is calculated using the MODFLOW. Considering the annual inflow volume from surrounding areas, it can be inferred that the inflow volume from the river network (blue path) in the Marvdasht-Kharameh aquifer has significantly decreased due to recent droughts.

Figure 5a shows the amount of water extracted by various exploitation sources (wells) within the study area's aquifer domain in different months. As can be seen from this figure, in the early months of the year, the amount of water exploited from the sources was much higher than in other months, and this trend has been almost stable for 8 years (2008 to 2016) or 127 months. Figure 5b illustrates the volume of in and outflow in the Marvdasht-Kharameh plain aquifer. As can be seen from the graph in Figure 5, with increased extraction from the aquifer in the study area, changes in the exchange volume of practical elements in the balance and a significant drop in the flow in the wells can be expected. Generally, according to Figure 5, it can be stated that the amount of water entering the area, in addition to being dependent on the physical conditions of the Marvdasht-Kharameh aquifer, such as hydrodynamic coefficients and gravity, directly depends on the pumping rate of the exploitation wells.

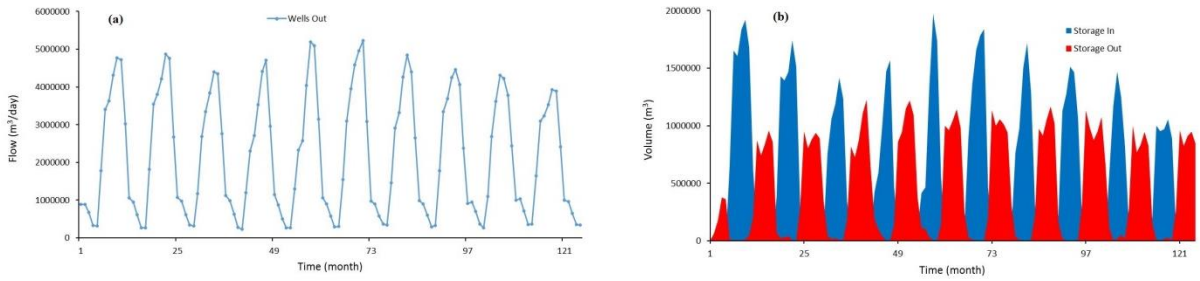

Figure 5. (a) Number of wells (flow out) and (b) The volume of water stored in the Marvdasht-Kharameh aquifer

279

280 **4.2. Model Output Water Level**

281 A model that has undergone calibration and validation is suitable for predicting the future state of the aquifer. It can
282 determine future conditions under desired stresses to improve performance and make management decisions. Figure
283 6 shows the groundwater level at the beginning of the 127-month analysis period for the study area aquifer and also
284 shows the groundwater level at the end of the analysis period (127 months), considering the ongoing extraction
285 (Figure 5a also shows this) from wells in the study area.

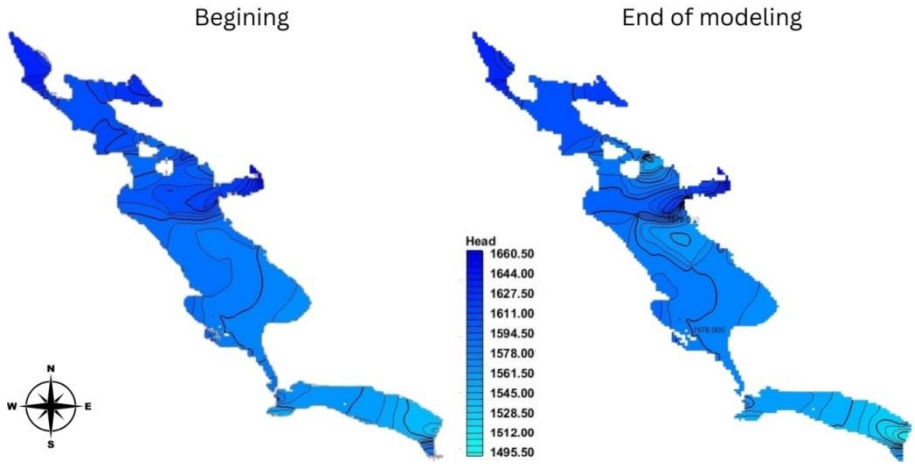

Figure 6. Groundwater level (m) of the Marvdasht-Kharameh aquifer for two periods, at the beginning and end (127 months), with continued extraction from wells.

286

287 In addition to the graphs shown in Figure 6, Table 3 summarizes the statistical status at the beginning and end of the
288 127 months in the study area aquifer.

289

290

291

Table 3. Summary of statistical head status at the beginning and end of the 127-month study period

Period	Min Value (m)	Max Value (m)	Range (m)	Mean (m)	Median (m)	Standard Deviation (m)
Beginning of Analysis	1533.19	1660.27	127.08	1589.35	1585.58	22.36
End of 127-Month Period	1506.88	1660.27	153.39	1581.68	1578.74	24.61

Considering the raster finite difference charts in Figure 6 and the statistical summary in Table 3, excessive groundwater extraction has decreased the water level in the Marvdasht-Kharameh aquifer over the approximately 11-year (127-month) study period.

Figure 7 represents a long-term prediction, extracted by applying restrictions and reducing extraction by 10% and 30% from the aquifer's exploitation sources, especially agricultural wells. These measures help stabilize the plain's hydrograph and prevent further groundwater level decline.

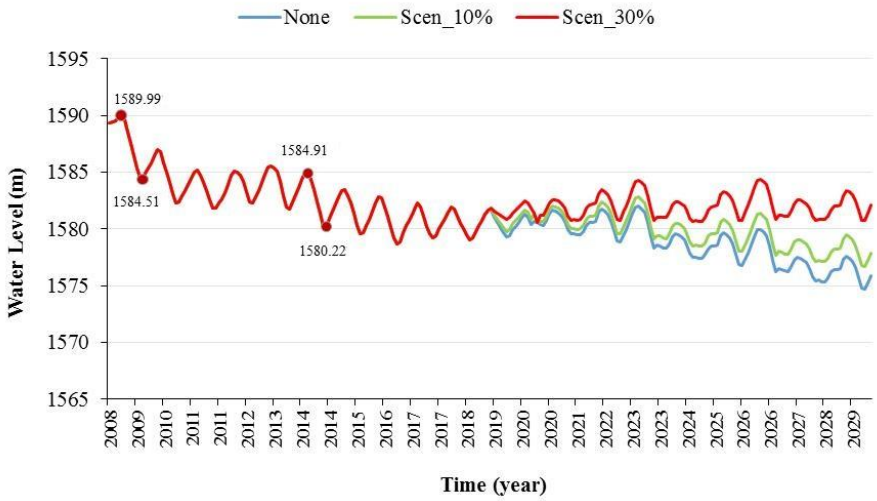

Figure 7. Unit hydrograph of the Marvdasht-Kharameh aquifer (finite difference network model output)

Based on the groundwater level map of the Marvdasht-Kharameh plain, the GMS software environment tools can be used to draw groundwater flow velocity and direction lines for the entire aquifer area according to the magnitude classification. The sudden drops at the four points are due to the 10% and 30% reduction in water extraction from the aquifer, particularly from agricultural wells. This initial decrease in extraction causes a temporary drop in the water level as the system adjusts to the new conditions. These drops represent the aquifer's response to the changes in water usage, which stabilizes over time, leading to a more sustainable groundwater level in the long run. As shown in Figure 8, the groundwater flow velocity in the middle parts of the aquifer is not too high. However, significant changes in direction can be observed in these areas. The highest velocity vectors are visible in the

boundary areas and near the porous borders. Thus, it can be stated that the drilling of numerous high-extraction wells in various parts of the aquifer has led to heterogeneous flow velocity structures within the Marvdasht-Kharameh plain.

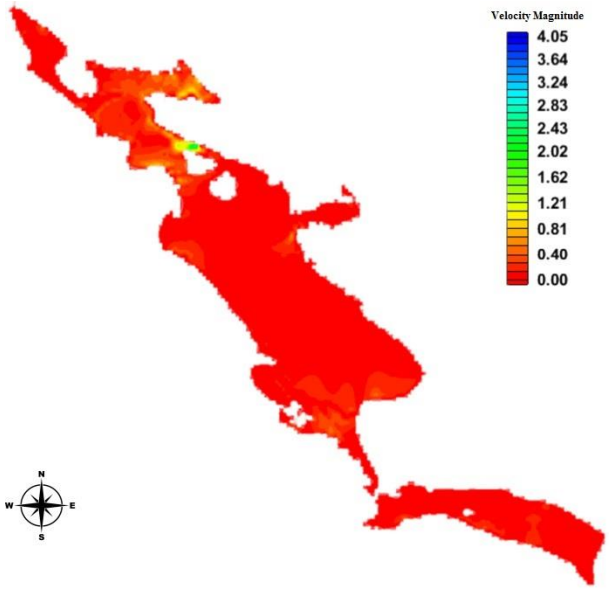

Figure 8. Velocity saturation of the final model of the Marvdasht-Kharameh aquifer

4.3. Determination of the Dispersion Coefficient in the Tracking Model

A drop in groundwater levels in an area can directly result in the infiltration of saline water from a wetland adjacent to an aquifer. Predicting future conditions of the Marvdasht-Kharameh aquifer suggests that the current decrease in groundwater levels may exacerbate these conditions. The MODFLOW model can forecast the unit hydrograph changes over a period equivalent to the simulation period (127 months). As previously mentioned, the increase in groundwater flow velocity in the aquifer can be influenced by artificial factors such as extraction sources or recharge elements like basins and injection wells, as well as the residual structure of the aquifer. This means that increased velocity in one area leads to a greater travel distance for particles (both saline and non-saline). The nature and structure of the groundwater reservoir, independent of natural barriers, significantly impact the dispersion coefficient.

Thus, the basis of uncertainty analysis calculations was derived from the dispersion coefficient analysis obtained from groundwater flow simulations in the Marvdasht-Kharameh plain. The dispersion coefficient is a key parameter for understanding the spreading of solutes, such as pollutants, within the groundwater flow system. The MODFLOW groundwater flow model was used to simulate water movement through the aquifer. The MODPATH

model was then employed to track the movement of particles, providing insight into the paths of solutes and their dispersion within the system. The dispersion coefficient was determined by analyzing these particles' travel distances and distribution over time. To estimate the dispersion coefficient more accurately, Kriging interpolation was applied to model the spatial distribution of particle movement across the aquifer, considering the heterogeneity of the system. Kriging helped create a more detailed spatial map of the dispersion coefficient by accounting for variations in particle movement at different locations within the aquifer. Additionally, First-Order Reliability Method (FORM) was used to perform uncertainty analysis, which refined the spatial variability of the dispersion coefficient and quantified the uncertainty associated with its estimation. This combined approach, utilizing MODPATH, Kriging interpolation, and FORM, enabled a more accurate determination of the dispersion coefficient, providing a deeper understanding of solute transport behavior in the aquifer and helping to assess potential contamination risks.

After optimizing calibration parameters in the finite difference model output and utilizing the MODFLOW mathematical model, water level elevations were generated for approximately eleven consecutive years following the initial month of stable simulation in the GMS software. Based on the results of Figure 6, primary coefficients in the MODPATH model were assigned to define the starting points for salinity analysis in all cells of the finite difference groundwater flow network. With only one starting point, this method's results represent particle paths across the plain.

In the next step, with the conversion of starting points to layering, spatial zonation was performed using the Kriging interpolation method in GIS software after determining the particle travel distances for each coordinate. The layer equation variogram setting and optimal parameter determination for the dispersion coefficient layer are shown in Figures 9. Figure 9 illustrates the local parameters set by the Kriging interpolation method. In this figure, the vertical axis represents semivariance (γ), a measure of the dissimilarity between pairs of data points as a function of the distance between them. Semivariance increases as the distance between points grows, indicating that data points farther apart become less similar or correlated. Essentially, it quantifies how much the data varies over space. The greater the semivariance, the less correlated the two data points are. The horizontal axis represents the distance (h) between pairs of data points in meters. It shows how the semivariance changes as the distance between the data points increases. The relationship between semivariance and distance helps to quantify the range of spatial correlation and is key for understanding the scale of spatial dependency in the dataset. The nugget refers to the value

of the semivariance at a distance of zero. This is the starting point of the curve and typically reflects measurement error or the inherent variability at very short distances. In the plot, the nugget is represented by the initial rise of the curve, often close to zero, which suggests minimal difference at very small distances.

The range is the distance at which the semivariance curve levels off and no longer increases significantly. Beyond this distance, the data points lose spatial correlation, indicating the effective distance over which spatial correlation exists. The sill represents the value where the semivariance curve flattens out. It is the upper limit of the semivariance, reflecting the total variability in the data that can be explained by spatial correlation. After reaching the range, the semivariance stabilizes at the sill, showing that spatial correlation is no longer significant.

The semivariogram models the spatial dependence between data points. Initially, as the distance between points increases, the semivariance also increases, showing that the correlation weakens with distance. Once the distance reaches the range, the semivariance stabilizes, indicating no further significant spatial correlation, which is represented by the sill. The nugget reflects short-range variability or measurement error. This relationship is crucial for understanding the spatial dependencies within the data and underpins geostatistical methods like kriging.

Additionally, the model shown in the semivariogram represents the fitted mathematical model that describes the spatial structure of the data. This model is fitted to the experimental data points (red dots), with the curve (blue line) representing the theoretical relationship between distance and semivariance. The binned points (red dots) represent the average semivariance calculated for specific distance intervals, and the averaged points (blue crosses) provide a smoothed version of the data for better visualization and model fitting.

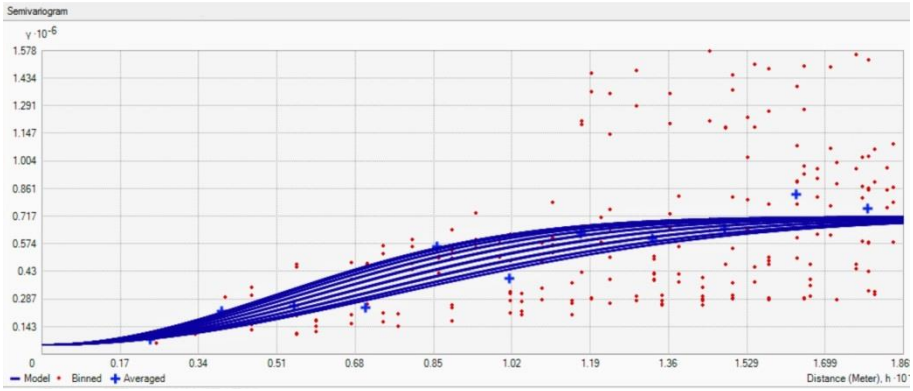

Figure 9. Parameters and variogram equation of zonation

According to Figure 9, when the distance between two points exceeds the range (1.869 m), the variogram's value approaches a constant value (0.71), indicating that the points are no longer spatially correlated. Also, a non-zero nugget effect indicates sudden changes at very small scales that larger-scale spatial models cannot explain. This indicates isotropy, meaning the spatial variability of dispersion is uniform in all directions. The error from the zonation process, if exceeding acceptable thresholds, will alter the extracted results heterogeneously.

According to the FORM theory, the dispersion coefficient layer was extracted as raster layers in sequential intervals based on the homogeneous magnitude (Figure 9). Overall, the particle paths for the same starting points were extracted in four main categories: 1, 32, 64 months, and the end period (127 months). These layers were finally converted into a matrix network using their cell values. The dispersion coefficient matrix was placed in the FORM method performance equation (Eq. 4) to determine the reliability, measuring the change in particle dispersion speed from the end of the period to the beginning.

To evaluate and analyze the spatial distribution of the transmissivity coefficient, a key parameter for groundwater exploitation, different geostatistical methods and distribution maps were compared using data from 240 deep wells (Figure 10).

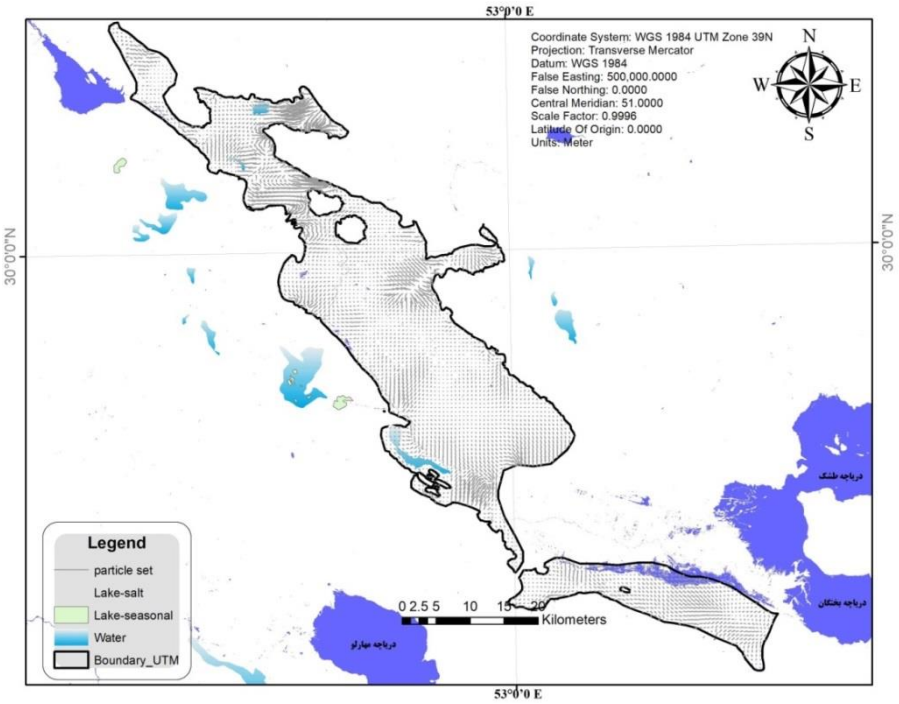

Figure 10. Transmissivity coefficient in the study plan at the end of the modeling period

For this purpose, the R^2 statistical parameter (Eq. 3) was used to evaluate these two methods. The results showed that the simple Kriging interpolation method with a correlation coefficient of 0.005 exhibits a good correlation. The

base value of the transmissivity coefficient, based on the path lengths obtained from the MODPATH model within the Marvdasht-Kharameh aquifer at the end of the simulation period, is shown in Figure 11. The fundamental assumption in preparing the function is to determine two periods of similar and independent lengths and to analyze changes in dispersion velocity considering the destruction of porosity in the final simulation period. It should be noted that the FP correlation coefficient is a statistical measure for evaluating the correlation between two nominal variables in a 2×2 contingency matrix, with a value ranging between -1 and 1, indicating the strength and direction of the relationship between two categorized variables.

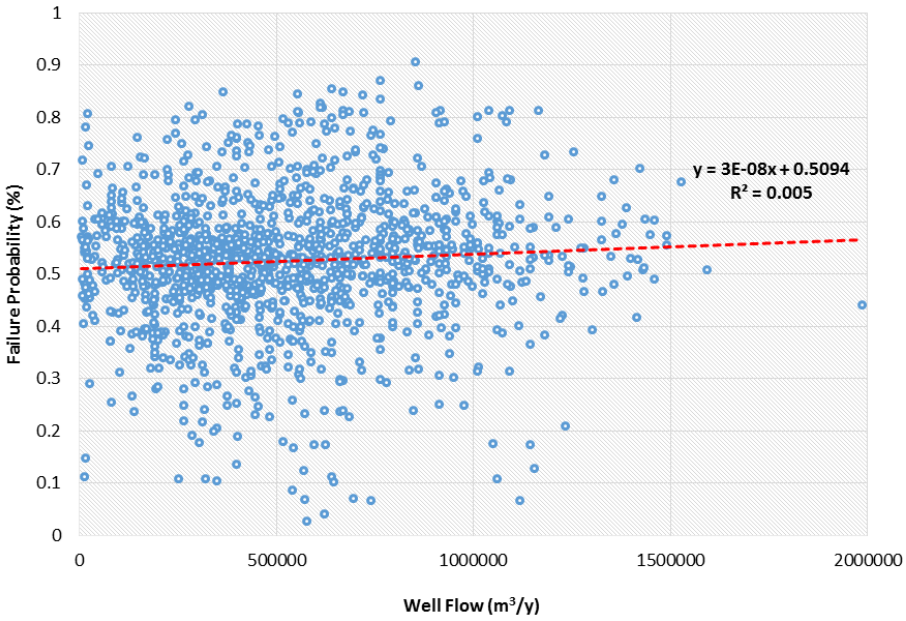

Figure 11. FP correlation coefficient and well discharge in the region

The very low correlation between the well discharge rates in the region and the failure coefficient at the exact coordinates, as shown in Figure 11, indicates that the determination of restricted areas to prevent aquifer formation destruction is not necessarily dependent on higher discharge rates.

The red dashed line in the plot represents a linear regression model that best fits the data. The slope of the line (3×10^{-8}) indicates that the change in well flow has a minimal effect on the failure probability. The R^2 value of 0.005 suggests that the model explains very little of the variation in the data, meaning the relationship between well flow and failure probability is not strong.

This study used reliability analysis methods, and probabilistic maps were extracted to identify the chances of transitioning from stable flow dispersion conditions (flow velocity and direction, temperature, pressure, medium

density) to areas prone to disruption of the stable groundwater flow in porous media. Figure 12 shows the position of saline water bodies relative to the saturated aquifer boundary. Assuming seasonal variations in the groundwater level of the plain and the saline water bodies, this study questioned the probability of salinity intrusion into the aquifer. The FORM method and its specific outputs highlight areas where groundwater levels decrease. Suppose the aquifer structure and natural gravitational flow directions are suitable. In that case, water from the identified saline bodies and wetlands will infiltrate the groundwater reservoir to compensate for the storage deficit.

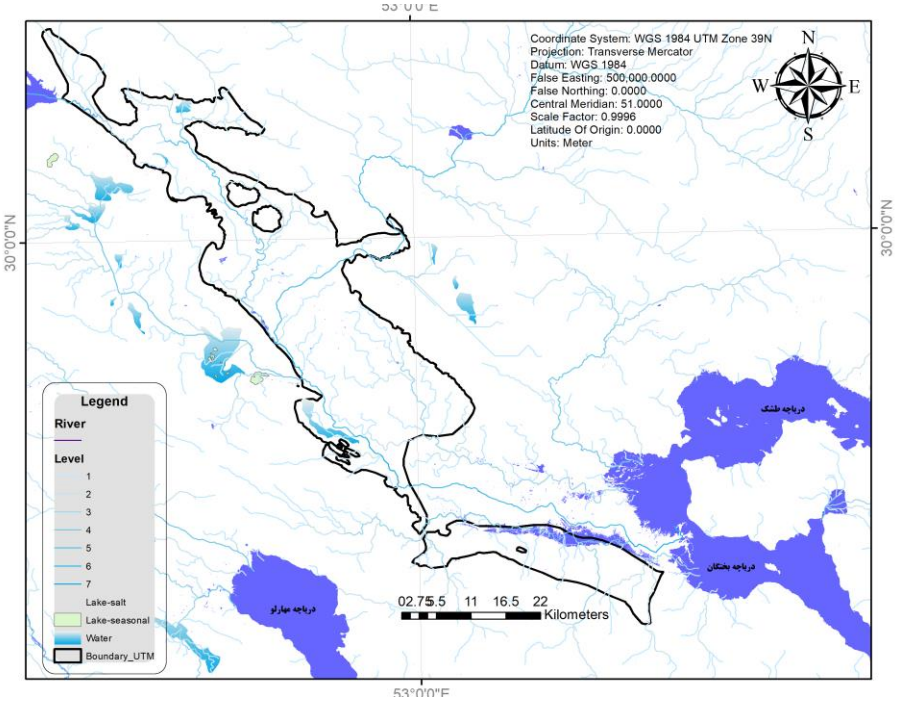

Figure 12. Position of saline water bodies relative to the saturated aquifer boundary.

The coefficients determined for all cells during the mentioned period were extracted using a linear regression equation in a spreadsheet environment, and the standard deviation was similarly calculated for 4035 cells. The importance function equation in the FORM method (Saghafian et al. 2021) is defined by Eq. (5):

$$G(x) = x_2 - x_1 \tag{5}$$

In this equation, x_2 represents the average value of the dispersion coefficient in each cell in the 95th month, and x_1 is the same value in the 32nd month. In other words, by executing the reliability analysis method's computational code, written in Python using the PyRe module, the final output, based on coordinates, allows for the creation of a continuous raster map zoned between each probable failure rate, where the percentage indicates the possibility of a reduction in the dispersion coefficient over the ten-year modeling period. Figure 13 also shows the beta index (β) of

failure probability (pink color) in the raster cells. This coefficient is highly consistent with the failure probability value in the numerical model's output. With a suitable estimation, the zonation can be represented as a raster layer, indicating the dispersion coefficient in the aquifer during the study period. In this study, "failure" refers to the probability that the groundwater flow system will undergo structural changes or degradation under given conditions, such as excessive groundwater extraction or salinity intrusion.

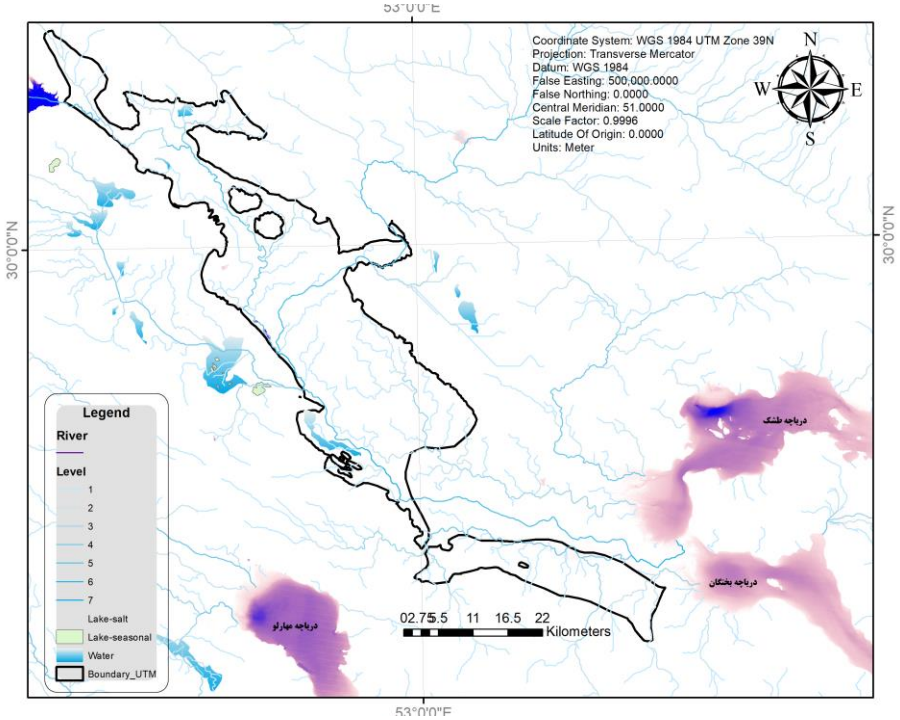

Figure 13. Occurrence percentage of saltwater bodies in front of a saturated aquifer

After preparing the matrix form of the diffusion coefficient layers in the inputs of the performance function equation and running the first-order reliability analysis method in the Python programming environment, the results are output as a matrix with maximum and minimum values of 6.98% and 0.011% for failure probability, respectively. As shown in Figure 3, determining restricted areas to prevent aquifer formation destruction is not necessarily dependent on higher discharge rates, and essential recharge parameters of the plain likely significantly impact flow displacement events. The failure probability in each case indicates the chance of flow path destruction in the raster cell of the study area. In Figure 3, the locations of areas with worse conditions in terms of tolerance against degradation and reduced water flow are shown in redder colors, according to the figure legend. The 50% probability indicates areas where structural changes will not cause significant damage to the flow network. Any value below 50% inversely represents the chance of failure. Classes above 50% should be considered highly sensitive, restricted

areas. However, simple zoning based on parametric interaction is impossible for groundwater management. The critical point is that the reduction zone for degradation, with decreasing density in the diffusion coefficient in areas where the probability of failure is calculated to be less than 50%, is practically meaningless against the concept that degradation in the flow layers is based on anthropogenic activities. In other words, although water accumulation in the groundwater layers in some areas increases with the overall degradation of the aquifer network, this water is extracted from the reservoir for local use, and with the continuation of current trends and considering pessimistic climatic conditions, it leads to changes in the flow expansion pattern. Here, the probability of failure in each case indicates the chance of structural failure in the raster layer cell of the study area.

According to the graph in Figure 14, it can be stated that in the Marvdasht-Kherameh aquifer, due to continuous withdrawals by multiple exploitation wells during ten years from 2006 to 2016 (127 month), as well as the extension of these conditions to the end of the hypothetical ten-year forecast period, and the potential for drilling illegal wells, climatic changes, and drought occurrence leading to aquifer system depletion, changes in the diffusion coefficient in the upcoming period will be very significant in some areas. The main reason for this is the high drop in groundwater levels, which will be lost based on the destruction of the alluvial aquifer structure and the blockage of a large portion of the voids that were considered the ultimate potential for water storage in the aquifer. The highest probability of failure, meaning the most significant reduction in the aquifer's diffusion coefficient, will occur precisely in areas previously identified as having high vulnerability based on three parameters: excessive drawdown, minimum exploitation wells, and the highest dispersion coefficient in the final map.

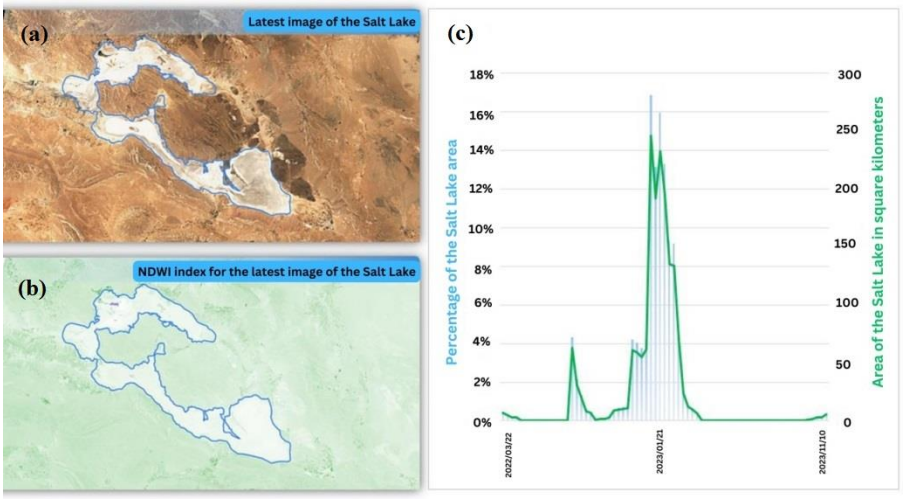

Figure 14. Time series of water availability in the wetlands of the investigated area in recent years. (a,b) latest image and NDWI index of salt lake and (c) percentage and area of the salt lake during time of study

One of the reasons for the unlikely infiltration of water into the aquifer is the lack of water sources within the wetland area. Figure 14 shows that, based on satellite images, the chance of water presence in parts of the wetland is less than 20%. Even in the best conditions, this value has not reached 100%. This situation has worsened in recent years. The satellite images on the left side of Figure 14 illustrate the changes in the Salt Lake's water coverage. The top photo shows the latest visible satellite image of the Salt Lake, outlining the current water boundaries. In contrast, the bottom image displays the NDWI (Normalized Difference Water Index) for the same region, highlighting areas with significant water coverage compared to dry land.

On the right side (Figure 14), the graph shows the time series data for two key metrics: the area of the Salt Lake in square kilometers (green line) and the percentage of the Salt Lake's area (blue line). The sharp fluctuations, especially in 2020 and 2021, with notable peaks, highlight the drastic changes in water availability in recent years. These spikes indicate heavy rainfall or sudden water inflow, which has not been consistent over time.

The green line (Figure 14), representing the area of the lake in square kilometers, shows the physical changes in the size of the lake, with notable increases during periods of significant rainfall, followed by sharp declines. The blue line, showing the percentage of Salt Lake's area, emphasizes the relative changes in water coverage compared to the total area. During peak water levels, the lake covered more than 16% of its location, but these levels have decreased substantially during dry periods, reflecting the reduction in water availability.

This situation is critical because the aquifer's water level also drops as the lake's water level decreases. Therefore, attention must not only focus on the aquifer's condition in terms of receiving water from surrounding areas but also on the potential of these water sources within the wetland itself. The decreasing water levels, both in the lake and the aquifer, point to a growing water scarcity problem, underlining the need for better water resource management to address the challenges faced by this region.

Based on the results of this study, it can be concluded that the inability to implement comprehensive scenarios, such as significantly reducing the extraction discharge of agricultural wells uniformly across the plain, highlights the importance of the saline water intrusion from surface water sources. The failure probability ranges from a maximum of 98% to a minimum of zero percent. The southern parts of the plain and the lower middle areas have a higher chance of maintaining the permeability structure. However, these areas are also critical in the flow of salinity. Considering that a decrease in the dispersion coefficient can be interpreted as a reduction in the aquifer's ability to transfer flow, the forward trend suggests the recurrent intrusion of saline flow towards the aquifer and, consequently,

481 the drying of the wetland. The highest risk areas are in the plain's middle parts, indicating long-term salt
482 accumulation in the infiltration area.
483
484 **5. Conclusions**
485 This study provides a comprehensive and detailed examination of the dynamics of groundwater in the Marvdasht-
486 Kherameh aquifer, with a particular focus on the interactions between freshwater and saline groundwater. Through
487 the application of advanced modeling techniques, such as MODFLOW and MODPATH, the study simulates the
488 movement and behavior of the mixing front under varying conditions, including groundwater extraction, seasonal
489 recharge, and the impact of human activities. By modeling these factors, we have been able to better understand how
490 the mixing front responds to changes in aquifer dynamics and to identify the most critical factors that influence
491 salinity intrusion into freshwater zones. The results offer significant insights into aquifer management strategies,
492 particularly in regions vulnerable to salinity intrusion and over-extraction of groundwater resources. The key
493 findings of this study include:
494 • Models revealed that groundwater extraction plays a pivotal role in shifting the mixing front towards freshwater
495 zones, particularly in high-risk regions where extraction rates are higher. This indicates the need for careful
496 management to avoid salinity intrusion, which could compromise freshwater resources.
497 • The behavior of the mixing front was found to be significantly influenced by seasonal variations in extraction
498 and recharge. During dry periods, when extraction rates peak, the mixing front extends more rapidly,
499 particularly in high-risk zones. On the other hand, regions with higher recharge rates showed more stability,
500 with less movement of the mixing front.
501 • The sensitivity analysis demonstrated that hydraulic conductivity, salinity levels, and recharge rates strongly
502 affect the dynamics of the mixing front. Variations in these parameters caused significant shifts in the location
503 of the mixing front, highlighting their crucial role in the behavior of groundwater and salinity intrusion.
504 • The study emphasizes the importance of sustainable groundwater management in preventing salinity intrusion
505 and ensuring the preservation of freshwater resources. Effective strategies include optimizing extraction rates,
506 artificial recharge, and strategic well placement to maintain a healthy balance between fresh and saline
507 groundwater.

- Although the study provides robust insights into the mixing front's behavior, there is a need for further research to incorporate real-time monitoring data into the models, allowing for more accurate and adaptive groundwater management. Additionally, expanding the sensitivity analysis to include more detailed field data on hydraulic parameters and salinity levels will improve the predictive accuracy of the models. Further exploration of advanced modeling approaches that consider non-uniform flow and complex geological conditions will also enhance our understanding of the aquifer's dynamics.

In conclusion, this research contributes significantly to the understanding of aquifer dynamics and offers practical guidance for managing groundwater resources in arid regions. By combining advanced modeling, real-time data, and sustainable extraction practices, future studies can improve water resource management strategies and contribute to the long-term sustainability of aquifers in areas vulnerable to salinity intrusion and over-extraction.

While this study provides valuable insights, future research should focus on several key areas to enhance groundwater management strategies. First, integrating real-time monitoring data into modeling can improve predictions of the mixing front's movement, enabling more responsive and dynamic management of the aquifer. Additionally, conducting a more detailed sensitivity analysis by incorporating parameters like hydraulic conductivity, salinity levels, and recharge rates will refine the models and optimize management practices.

Future work should also explore advanced modeling techniques to account for non-uniform flow and aquifer heterogeneity, improving predictions in complex geological conditions. Moreover, investigating sustainable extraction practices, such as artificial recharge and well optimization, is essential to prevent salinity intrusion and ensure the long-term health of the aquifer. Lastly, considering the impact of climate change on groundwater dynamics will be crucial, as changing precipitation and temperature patterns could alter the behavior of the mixing front.

Declaration

Ethics approval and consent to participate

Not applicable

Consent for publication

Not applicable

Competing Interest

The authors declare that they have no known competing financial interests or personal relationships that could have appeared to influence the work reported in this paper.

Funding / Grant Information

This work was supported by the Ferdowsi University of Mashhad (grant number FUM-3/60921).

Acknowledgements

We would like to thank all the participants in this study for their time and willingness to share their experiences.

Author contributions

All authors contributed to the study's conception and design. Shahin Tavallali, Mahmoud F. Maghrebi, and Mohammad Taghi Dastorani performed material preparation, data collection, and analysis. Shahin Tavallali wrote the first draft of the manuscript, and all authors commented on previous versions. All authors read and approved the final manuscript.

Availability of data and material

The data will be made available at a reasonable request.

References

Ahani, H., Noshadi, M.: Application of cadastre maps, agricultural database and MODIS satellite images for monitoring cultivated areas. *Iranian Journal of Science and Technology, Transactions of Civil Engineering*, ***43***, 179-192 (2019).

Ahmadi Akhormeh, M., Nohegar, A., Soleimani Motlagh, M., Taie Samiromi, M.: Groundwater Drought Investigating using SWI and GRI Indices) Case Study: Marvdasht Kharameh Aquifer). *Irrigation and Water Engineering*, *6*(1), 105-118 (2015).

Akter, A., Ahmed, S.: Modeling of groundwater level changes in an urban area. *Sustainable Water Resources Management*, *7*, 1-20 (2021).

Alaviani, F., Sedghi, H., Asghari Moghaddam, A., Babazadeh, H.: Adopting GMS–PSO model to reduce groundwater withdrawal by integrated water resources management. *International Journal of Environmental Research*, *12*, 619-629 (2018).

Ali, G., Maghrebi, M. F.: Modifications to the single point velocity measurement method for estimating river discharge in low-resource environments. *Journal of Hydraulic Engineering*, *149*(11), 06023008 (2023).

Alimonti, C., Lombardi, M., Cardarilli, M., Soldo, E.: Reliability Analysis Applied on Land Subsidence Effects of Groundwater Remediation: Probabilistic vs. Deterministic Approach. *Water Resources Management*, *31*, 1745-1758 (2017).

Amanambu, A. C., Obarein, O. A., Mossa, J., Li, L., Ayeni, S. S., Balogun, O., Ochege, F. U.: Groundwater system and climate change: Present status and future considerations. *Journal of Hydrology*, *589*, 125163 (2020).

Amiri, S., Rajabi, A., Shabanlou, S., Yosefvand, F., Izadbakhsh, M. A.: Prediction of groundwater level variations using deep learning methods and GMS numerical model. *Earth Science Informatics*, *16*(4), 3227-3241 (2023).

Ayar, P., Baradaran, S., Abdipour Vosta, S.: A review on the effect of various additives on mechanical properties of stone mastic asphalt (SMA). *Road*, *30*(110), 57-86 (2022).

Baradaran, M. S., Aftabi Sani, A., Abrishami, S.: Application of Differential Transform Method for Solving Free-Surface Seepage Problem of One-Dimensional Porous Media. *Ferdowsi Civil Engineering*, *37*(1), 1-18 (2024).

Baradaran, S., Ameri, M.: Investigation of rutting failure in asphalt mixtures and its improvement strategies. *Road*, *31*(114), 53-70 (2023).

Bonì, R., Meisina, C., Teatini, P., Zucca, F., Zoccarato, C., Franceschini, A., Herrera, G.: 3D groundwater flow and deformation modelling of Madrid aquifer. *Journal of Hydrology*, *585*, 124773 (2020).

Cao, F., Jaunat, J., Vergnaud-Ayraud, V., Devau, N., Labasque, T., Guillou, A., Ollivier, P.: Heterogeneous behaviour of unconfined Chalk aquifers infer from combination of groundwater residence time, hydrochemistry and hydrodynamic tools. *Journal of Hydrology*, *581*, 124433 (2020).

Dey, S., Prakash, O.: Pumping Optimization for Saltwater Intrusion Management in a Coastal Aquifer with Combined Use of Sharp Interface and Density Dependent Models. In *Groundwater and Water Quality: Hydraulics, Water Resources and Coastal Engineering,* 287-301 (2022).

Doherty, J.: PEST-ASP user's manual. *Watermark Numerical Computing, Brisbane, Australia* (2001).

Feo, A., Zanini, A., Petrella, E., Celico, F.: A Python script to compute isochrones for MODFLOW. *Groundwater*, *56*(2), 343-349 (2018).

Ghandehari, Y., Nouri, A. Z., Aminnejad, B.: Assessment of contamination dispersion in a porous aquifer environment using explicit and implicit methods in the MODFLOW–MODPATH model. *Applied Water Science*, *14*(5), 1-16 (2024).

Heydari, A., Jabbari, I.: Simulation of Marvdasht groundwater level and investigation of forecast scenarios using MODFLOW mathematical code. *Hydrogeomorphology*, *8*(29), 172-149 (2022).

Hu, Y., Ji, J., Sun, Z., Dias, D.: First order reliability-based design optimization of 3D pile-reinforced slopes with Pareto optimality. *Computers and Geotechnics*, *162*, 105635 (2023).

Iqbal, J., Nazzal, Y., Howari, F., Xavier, C., Yousef, A.: Hydrochemical processes determining the groundwater quality for irrigation use in an arid environment: the case of Liwa Aquifer, Abu Dhabi, United Arab Emirates. *Groundwater for Sustainable Development*, *7*, 212-219 (2018).

Liu, X., Gong, M., Zhou, Z., Xie, J., Wu, W.: An improved first order approximate reliability analysis method for uncertain structures based on evidence theory. *Mechanics Based Design of Structures and Machines*, *51*(7), 4137-4154 (2023).

Ma, C., Shi, W., Zhan, H.: Estimating hydraulic diffusivity in coastal confined aquifer under tidal fluctuation using a frequency domain model. *Journal of Hydrology*, 131421 (2024).

Mohammadi, Z., Illman, W. A., Field, M.: Review of laboratory scale models of karst aquifers: approaches, similitude, and requirements. *Groundwater*, *59*(2), 163-174 (2021).

Vatanchi, S. M., Maghrebi, M. F.: Uncertainty Analysis of Stage-Discharge Rating Curves In Rivers. *Journal of Civil and Environmental Engineering*, *52*(106), 157-167 (2022).

Mohammed, K. S., Shabanlou, S., Rajabi, A., Yosefvand, F., Izadbakhsh, M. A.: Prediction of groundwater level fluctuations using artificial intelligence-based models and GMS. *Applied Water Science*, *13*(2), 54 (2023).

Mokarram, M., Pourghasemi, H. R., Huang, K., Zhang, H.: Investigation of water quality and its spatial distribution in the Kor River basin, Fars province, Iran. *Environmental Research*, *204*, 112294 (2022).

Moutsopoulos, K. N.: A simple model for the simulation of the flow behavior in unconfined double porosity aquifers. *Journal of Hydrology*, *596*, 126076 (2021).

Pargar, J., Akhtarpour, A., Baradaran, M. S.: An Unsaturated Soil Mechanics-Based Numerical and Experimental Method to Assess Soil Settlement Due to Ground Water Level Rise. *Transportation Infrastructure Geotechnology*, 1-26 (2024).

Raja, O., Parsinejad, M.: Cost-effective strategies to improve crop water productivity—case study: Bakhtegan and Maharloo, Iran. *International Journal of Environmental Science and Technology*, *20*(1), 883-894 (2023).

Raja, O., Parsinejad, M., Sohrabi, T., Ahmadaali, K.: Status investigation of the marvdasht-kharameh water resources using sustainability analysis indicators. *Iranian Journal of Soil and Water Research*, *50*(4), 897-909 (2019).

Roy, D. K., Datta, B.: Modelling and management of saltwater intrusion in a coastal aquifer system: A regional-scale study. *Groundwater for sustainable development*, *11*, 100479 (2020).

Saghafian, B., KhanAhmadi Bafghi, H., Daneshkar Arasteh, P.: Forecasting the Area of the Bakhtegan and Tashk Lake Using Remote Sensing and Climatic Factors. *Iran-Water Resources Research*, *17*(1), 151-165 (2021).

Samani, S.: Unraveling aquifer dynamics: Time series evaluation for informed groundwater management. *Groundwater for Sustainable Development*, *25*, 101174 (2024).

627 Sharma, R., Kumar, R., Agrawal, P. R., Gupta, G.: Groundwater extractions and climate change. In *Water*
628 *conservation in the era of global climate change,* 23-45 (2021).

629 Tareghian, B., Baradaran, M. S., Akhtarpour, A.: The effect of sand-crumb rubber mixture treatment on the seismic
630 response of a low-rise building located on liquefiable soil. *Discover Geoscience*, *2*(1), 11 (2024).

631 Yazdi, A. N., Akhtarpour, A., Abdalhusein, M. M., Baradaran, M. S.: Experimental investigation of the volume
632 change of a swelling clay and its improvement. *Transportation Infrastructure Geotechnology*, *11*(3), 1008-1031
633 (2024).

634 Zhang, P., Aagaard, P., Gottschalk, L.: Probability method used in predicting contaminant risk in groundwater
635 adjacent to airport. *Water, Air, & Soil Pollution*, *211*, 323-339 (2010).